AGU PUBLICATIONS

Paleoceanography

RESEARCH ARTICLE
10.1002/2016PA002987

Key Points:
- Middle Miocene paleo-ocean circulation is sensitive to the position of the shelf break in the Weddell Sea
- Relative to a standard Miocene model bathymetry, a southerly placed shelf break in the Weddell Sea causes enhanced deep water formation
- Sensitivity of southern source water component to CO_2 changes depends on the position of the shelf break

Correspondence to:
X. Huang and M. Stärz,
Xiaoxia.huang@awi.de;
michael.staerz@awi.de

Citation:
Huang, X., M. Stärz, K. Gohl, G. Knorr, and G. Lohmann (2017), Impact of Weddell Sea shelf progradation on Antarctic bottom water formation during the Miocene, *Paleoceanography*, *32*, 304–317, doi:10.1002/2016PA002987.

Received 8 JUN 2016
Accepted 13 MAR 2017
Accepted article online 5 MAR 2017
Published online 31 MAR 2017

Impact of Weddell Sea shelf progradation on Antarctic bottom water formation during the Miocene

Xiaoxia Huang[1], Michael Stärz[1], Karsten Gohl[1], Gregor Knorr[1], and Gerrit Lohmann[1]

[1]Alfred Wegener Institute, Helmholtz-Centre for Marine and Polar Research, Bremerhaven, Germany

Abstract The Weddell Sea is a main location of bottom water formation and, thus, an important component of global ocean circulation. In this study we examine the ocean and climatic responses to a shelf progradation induced by ice sheet advance and glacially transported sediments during the Miocene, using a general circulation model. Our investigations show that relative to a Miocene standard bathymetry, a farther southerly placed shelf break, as reconstructed in a state-of-the-art bathymetry for the Weddell Sea, enables enhanced Antarctic Bottom Water (AABW) formation and gyre transport during the middle Miocene for both relatively high and low atmospheric CO_2 concentrations. Furthermore, CO_2 sensitivity experiments show that an atmospheric CO_2 decline for a setup with the southerly placed shelf break of a new bathymetry has only a minor impact on AABW formation, while the standard setup shows an increase. In combination, these impacts may explain the pronounced deep water formation in the southern high latitudes from the middle Miocene to the late Miocene.

1. Introduction

Geological proxy records, including global stacks of benthic of $\delta^{18}O$ and $\delta^{13}C$ (Figure 1), indicate a climate transition from a phase of relatively warm global conditions prior to the Middle Miocene Climatic Transition (pre-MMCT, 17–15 Ma) into a cooler climate mode during the late Miocene (11.6–5.3 Ma). The pre-MMCT is also an interesting period of global warmth with above-present temperatures, relatively high CO_2, and a substantially reduced Antarctic Ice Sheet [*Zachos et al.*, 2008; *You et al.*, 2009; *Mudelsee et al.*, 2014]. Average global temperature in the pre-MMCT was ~6°C warmer than present with reduced equator-to-pole thermal gradients [*Flower and Kennett*, 1994; *Shevenell et al.*, 2004]. The long-term cooling trend is superposed by a pronounced ice sheet growth in Antarctica, which represents the final step toward persistent large-scale glaciation with modern levels of Antarctic ice volume [*Langebroek et al.*, 2009, 2010] during the Middle Miocene Climate Transition (MMCT) beginning at ~14 Ma (Figure 1). Different hypotheses have linked these changes to alterations of tectonic gateways [*Woodruff and Savin*, 1989, 1991; *Raymo*, 1994; *Ramsay et al.*, 1998] and atmospheric CO_2 variations [*Dutton and Barron*, 1997; *Pagani et al.*, 1999] in conjunction with insolation changes [*Holbourn et al.*, 2005].

The middle to late Miocene interval is believed to represent a time of significant ice sheet expansion on Antarctica [*Shevenell et al.*, 2004; *Miller et al.*, 2005]. The stable isotope record of the deep sea demonstrates a strong enrichment in oceanic $\delta^{18}O$ and climatic cooling over 6 Ma during the middle Miocene times [*Zachos et al.*, 2008]. During this interval, the East Antarctic Ice Sheet is thought to have been a major and permanent ice sheet, despite fluctuations in its size [*Westerhold et al.*, 2005]. Furthermore, seismic stratigraphic data from the Ross Sea reveal major intervals of grounded ice advance and retreat, suggesting the presence of a large and dynamic West Antarctic Ice Sheet in the middle Miocene [*Bart*, 2003; *Chow and Bart*, 2003]. Estimates of the magnitude of Antarctic ice growth and temperature change during the middle Miocene climate reorganization have been established by using $\delta^{18}O$ covariance of benthic/planktonic foraminifers, foraminiferal Mg/Ca contents, sequence stratigraphy, and meridional stable isotope gradients [*Flower and Kennett*, 1994; *Lear et al.*, 2015]. Although these methods provide useful approximations of the relative contributions of ice volume and temperature with respect to the middle Miocene $\delta^{18}O$ signal, none involve a truly independent measure of either deep water temperature or ice volume.

Accompanying Antarctic cooling is thought to promote the production of AABW [*Hall et al.*, 2003], analogous to Southern Component Water (SCW), which forms mainly in the Weddell Sea and Ross Sea around the Antarctic continent. AABW has been identified as the densest water masses in the deep ocean since the middle Miocene [*Kennett et al.*, 1975]. Comparison of benthic carbon and oxygen isotope data used as

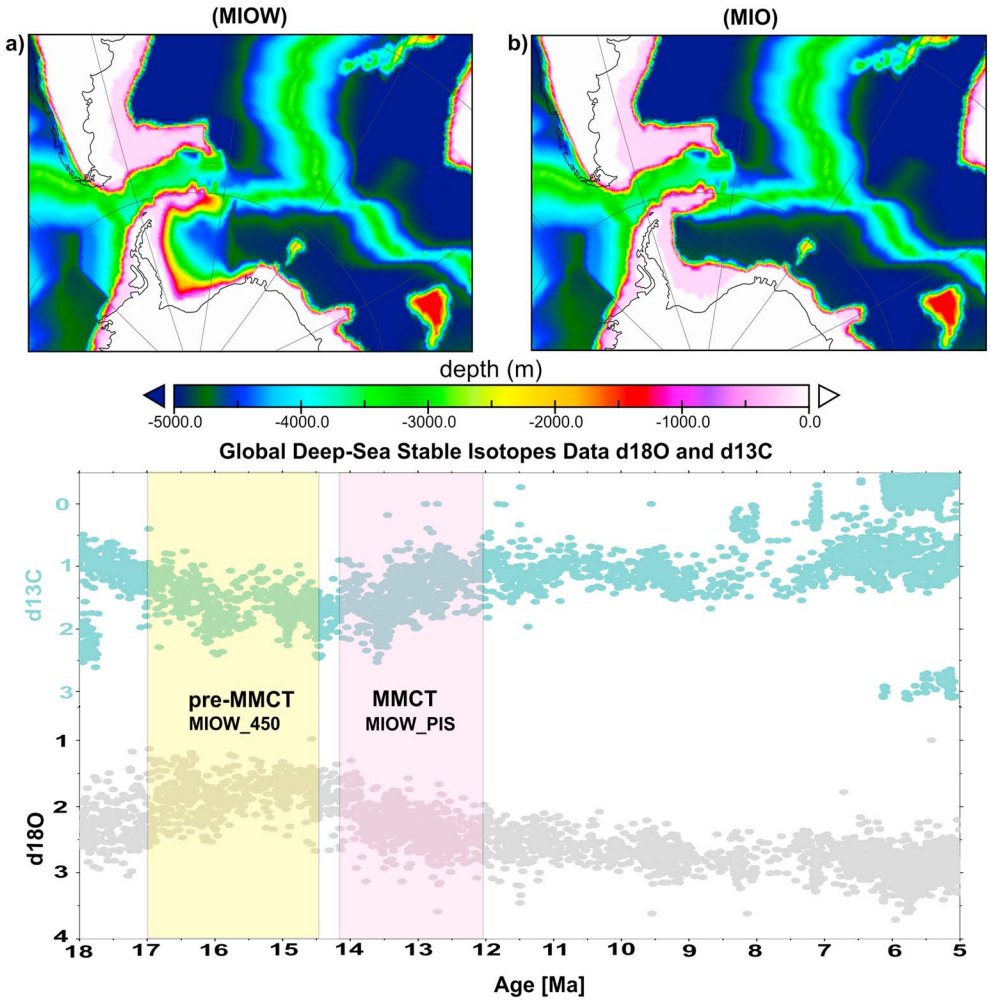

Figure 1. Two recent reconstructed paleobathymetries are applied in the model simulations to test their impacts on the ocean circulation (a) by *Huang et al.* [2014] and (b) by *Herold et al.* [2008]. $\delta^{18}O$ and $\delta^{13}C$ plots indicate the possible correlation between model simulation and time period.

paleotracers from the Atlantic, Indian, Pacific and Southern Oceans initially provided evidence that the AABW was the dominant source of deep water through the middle Miocene, whereas North Atlantic Deep Water (analogous to Northern Component Water) formation remained weak until ~12 Ma [*Woodruff and Savin*, 1989, 1991; *Wright et al.*, 1991; *Flower and Kennett*, 1994]. Furthermore, a strengthening of AABW formation has been inferred from silt analyses that show long-term changes in flow speed of the AABW entering the Pacific [*Hall et al.*, 2003] between ~15.5 and ~13.5 Ma. In order to explain changes in the intensity of AABW formation, modeling studies have mainly focussed on the impact of CO_2 and ice sheet variations [e.g., *Knorr and Lohmann*, 2014; *Goldner et al.*, 2014], alterations in different gateway configurations, and paleogeography [e.g., *Hamon et al.*, 2013; *Kennedy et al.*, 2015].

Herein, we focus on an alternative modeling approach that investigates the long-term impact of shelf progradation due to massive glacial sediment deposition. Such a progressive shelf expansion of the outer shelves is well observed from seismic data and stratigraphy around the Antarctic margins [e.g., *Cooper et al.*, 2008; *Gohl et al.*, 2013; *Huang et al.*, 2014], leading to large-scale geomorphic features (trough fans and contourite drifts) on the continental rise that point to massive sediment transport processes by ice sheet advances on the shelf with intensified bottom current activities in the Miocene [e.g., *Rebesco et al.*, 1997; *Uenzelmann-Neben and Gohl*, 2012; *Huang and Jokat*, 2016a, 2016b]. On the southern Weddell Sea continental rise, about two thirds of the sediment thickness were already in place by the latest Miocene [*Huang et al.*, 2014].

In spite of the constraints for AABW formation history, understanding the underlying mechanisms depends on a complex interplay of ice sheet expansion, atmospheric CO_2 concentration, and paleobathymetric conditions. In contrast to previous coupled model simulation results in which the AABW formation was mainly forced by a decrease in atmospheric CO_2 and ice sheet expansion during the middle Miocene, we hypothesize that a pronounced shelf progradation along the southern margin of the Weddell Sea might have controlled ocean circulation and formation of AABW via a long-term impact during the middle Miocene to late Miocene interval. This hypothesis is tested with a fully coupled atmosphere-ocean general circulation model (GCM) by implementing a newly reconstructed paleobathymetry of the Weddell Sea region (Figure 1) [*Huang et al*., 2014]. Furthermore, the superposed effects of ice sheet and CO_2 changes on shelf progradation have also been taken into account to evaluate the importance of different forcing mechanisms for the Miocene climate evolution in dependence of the shelf break position in the Weddell Sea.

2. Data and Methods

The middle Miocene model setup applies a global paleobathymetry, orography, and ice sheet adjustments [*Herold et al*., 2008] and is updated by the regional paleobathymetry encompassing the North Atlantic/Nordic Seas sector [*Ehlers and Jokat*, 2013]. We further embed the new paleobathymetry (Figure 1) of the Weddell Sea sector [*Huang et al*., 2014] into the standard middle Miocene model setup (MIOW). The new paleobathymetry of the Weddell Sea by *Huang et al*. [2014] for the Miocene was generated by removing sediment thicknesses for the past 15 Ma (up to 5 km) based on all available seismic data, velocity-depth functions, and chronostratigraphic information from drill sites [*Barker et al*., 1988; *Smith and Anderson*, 2011], followed by a backstripping procedure. The southern Weddell Sea continental slope and rise in the new paleobathymetry grids demonstrate a more southerly placed deepening trend, which we utilized as the middle Miocene paleobathymetric boundary condition. It differs largely from the Weddell Sea segment of the global approach by *Herold et al*. [2008]. They generally defined a mean sediment thickness of 270 m above oceanic basement for the past 15 Ma, which shows a broad flat shelf in the southern Weddell Sea due to lacking constraints from seismic records (Figure 1b).

The Miocene climate and ocean circulation is investigated by means of the fully coupled global atmosphere-ocean-sea ice-vegetation Earth System Model COSMOS, originally developed at Max Planck Institute in Hamburg [*Jungclaus et al*., 2006]. The atmospheric model ECHAM5 (European Centre/Hamburg) [*Roeckner et al*., 2003], complemented by a land surface component JSBACH [*Brovkin et al*., 2009], is used at T31 resolution (~3.75°), with 19 vertical layers. The ocean model MPIOM [*Marsland et al*., 2003], including thermal dynamics that is formulated using viscous-plastic rheology, has a mean resolution of GR30 ($3° \times 1.8°$) in the horizontal, with 40 uneven vertical layers. The climate model has already been used to simulate the last millennium [*Jungclaus et al*., 2010], the Holocene, the Last Glacial Maximum, and the Miocene warm climate [*Knorr et al*., 2011; *Wei and Lohmann*, 2012; *Lohmann et al*., 2013; *Gong et al*., 2013; *Zhang et al*., 2014; *Knorr and Lohmann*, 2014; *Stärz et al*., 2016; *Stein et al*., 2016].

In addition to the paleotopography, the standard Miocene model setup includes changes in greenhouse gases and land surface characteristics with respect to present day. More explicitly, land surface characteristics, like vegetation changes, are directly modeled by JSBACH and more realistic physical soil properties (total water holding field capacity of soils and soil albedo) are taken into account by inferring soil parameters [*Stärz et al*., 2016] from a late Miocene vegetation reconstruction [*Micheels et al*., 2007]. Within a set of model experiments (Table 1), we use preindustrial levels (278 ppmv) and relatively high levels of atmospheric CO_2, (450 ppmv), which are placed well within the uncertainty of CO_2 reconstructions, ranging between atmospheric concentrations less than 280 and more than 550 ppmv [e.g., *Pagani et al*., 2005; *Beerling and Royer*, 2011].

A complete list of the model experiments, including sensitivity studies with different atmospheric CO_2 levels, present-day and reduced (approximately −300 m) Antarctic Ice Sheet height configurations, and Weddell Sea bathymetry data sets [*Herold et al*., 2008; *Huang et al*., 2014], is given in Table 1. The standard model experiments MIO_278, MIO_450, and MIOW_450 are initialized from three-dimensional present-day ocean temperature and salinity fields and are run >4000 years into equilibrium. Thereafter, ocean salinity and temperature fields are taken from the respective model experiments in order to initialize model runs MIOW_278

Table 1. The List of Modeling Experiments With Their Boundary Conditions[a]

Model Runs	Atmospheric CO_2 (ppmv)	Paleobathymetry	Ice Sheet Height	Length of Simulation (Model Years)	Time Slices
MIO_450	450	Miocene[b]	reduced[b]	4000	
MIOW_450	450	Miocene including reconstruction of the Weddell Sea[c]	reduced	4000	**Pre-MMCT (17–15 Ma)**
MIOW_278	278	Miocene including reconstruction of the Weddell Sea	reduced	1200	
MIOW_PIS	278	Miocene including reconstruction of the Weddell Sea	present day	1200	**MMCT (14–12 Ma)**
MIO_278	278	Miocene[b]	reduced	4200	
MIO_PIS	278	Miocene[b]	present day	1000	

[a]Boldface is applied to highlight the interested time slices.
[b]*Herold et al.* [2008].
[c]*Huang et al.* [2014].

and MIOW_PIS, which have been integrated for another 1200 model years. The final 100 years of simulation of each model experiment are taken for analysis.

3. Results

3.1. Effect of Shelf Break Location for High CO_2 Level and a Low Ice Sheet

By means of fully coupled global atmosphere-ocean GCM, we examined the isolated impacts of the shelf break migration at high CO_2 level of 450 ppmv to capture essential feedbacks in a warm climate simulation that is representative of the middle Miocene. Whereas the standard model experiment MIOW_450 (Figure 2a) (atmospheric CO_2: 450 ppmv) includes a southerly placed shelf break, MIO_450 applies a more northward

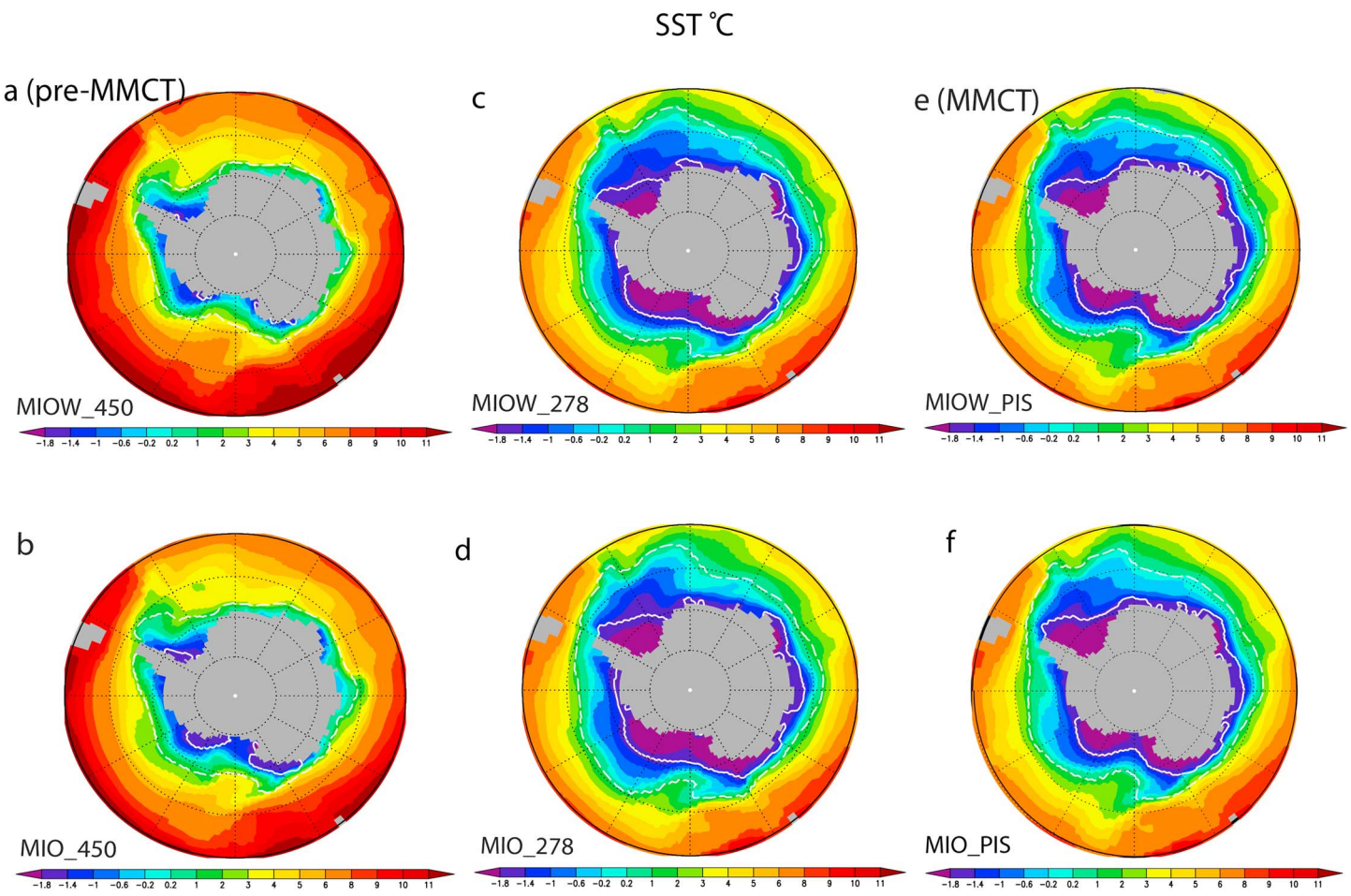

Figure 2. Simulated sea surface temperature (SST in °C) for five model experiments (MIOW_450, MIO_450, MIOW_278, MIO_278, MIOW_PIS, and MIO_PIS). The dashed line of sea ice extent reflects 15%.

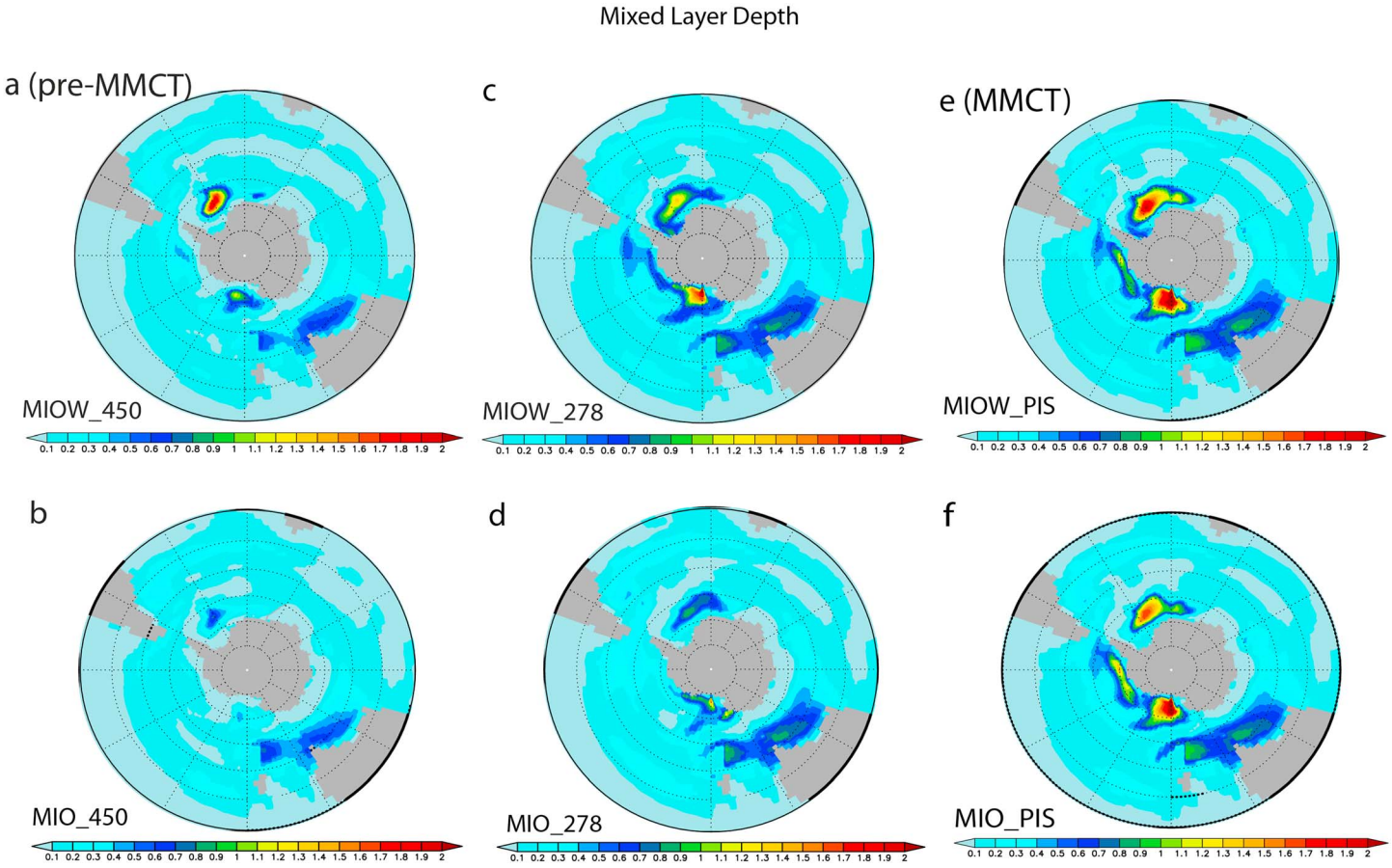

Figure 3. Simulated sea surface temperature (SST in °C) for six model experiments (MIOW_450, MIO_450, MIOW_278, MIO_278, MIOW_PIS, and MIO_PIS).

migrated shelf break location that roughly corresponds to the present-day location in the southern Weddell Sea. The standard model experiment MIOW_450 provides warming at the sea surface in combination with reduced perennial sea ice extent in the southern Weddell Sea with respect to simulation MIO_450 (Figures 2a and 2b). Thereby, a southerly placed shelf break induces sea surface temperature (SST) changes occurring at the Weddell Sea and Ross Sea sectors that are up to 6°C warmer than the preindustrial model simulation (not shown). In MIO_450, however, which is characterized by a north migrated shelf break, the Ross Sea and southwest of the Weddell Sea still show limited perennial sea ice cover and SSTs close to the freezing point (Figure 2b). Apart from the modeled temperature and sea ice conditions, the model experiments further provide insight into the mixed layer depth and velocity of the gyre circulation in the Weddell Sea with the different bathymetric constraints. With respect to MIO_450, MIOW_450 shows a distinct deepening of the mean mixed layer depth (Figures 3a and 3b) in the Weddell Sea that extends to the seafloor during austral winter and is coupled to an intensified Weddell Gyre that extends from surface to deep water levels (Figures 4a, 5a, and 6a). By applying a southerly displaced Weddell Sea shelf break (MIOW_450), the center of the Weddell Gyre, defined by the minimum of dynamic topography [*Hayes et al.*, 2009], shifts ~6° poleward (preindustrial: 61.5°S; MIO_450: 60.5°S; MIOW_450: 66.5°S) (Figures 4a, 4b, 5a, and 5b). In both experiments (Figures 5a and 5b) the subsurface circulation (37 m) is significantly intensified compared to preindustrial and a pronounced deep water circulation (3070 m) of the Weddell Sea is shown near the southeast coast and northwest coast of the Weddell Sea (Figure 6a). For MIO_450 instead, this gyre circulation largely decreases or partly vanishes along the west coast of the Weddell Sea in the deep water levels (Figure 6b).

In Figures 7 and 8, the modeled large-scale ocean circulation is presented as the Global Meridional Overturning Circulation (GMOC) and the Atlantic Meridional Overturning Circulation (AMOC). Therein, the global AABW of MIOW_450 increases up to −6.5 sverdrups (Sv) as compared to MIO_450 (Figure 7a and Table 2). In the Atlantic sector, enhanced inflow of AABW reaches 40°N and is observed at depth levels

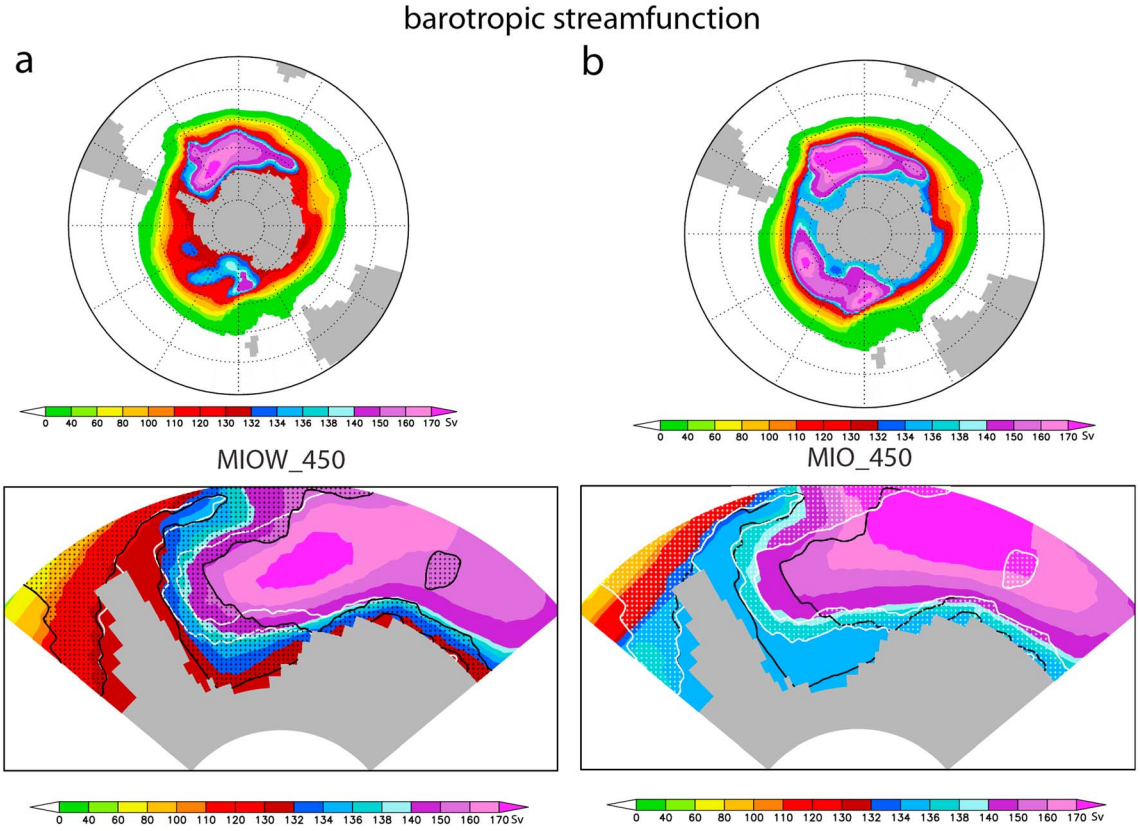

Figure 4. Barotropic stream function (MIOW_450 and MIO_450). (a and b) The 3000 m and 1000 m model depth contour lines are drawn to show the bathymetry slope of MIOW_450 in white and MIO_450 in black. The dotted area highlights the slope that has been used in the respective model simulation (sverdrup: $Sv = 1 \times 10^6\ m^3/s$).

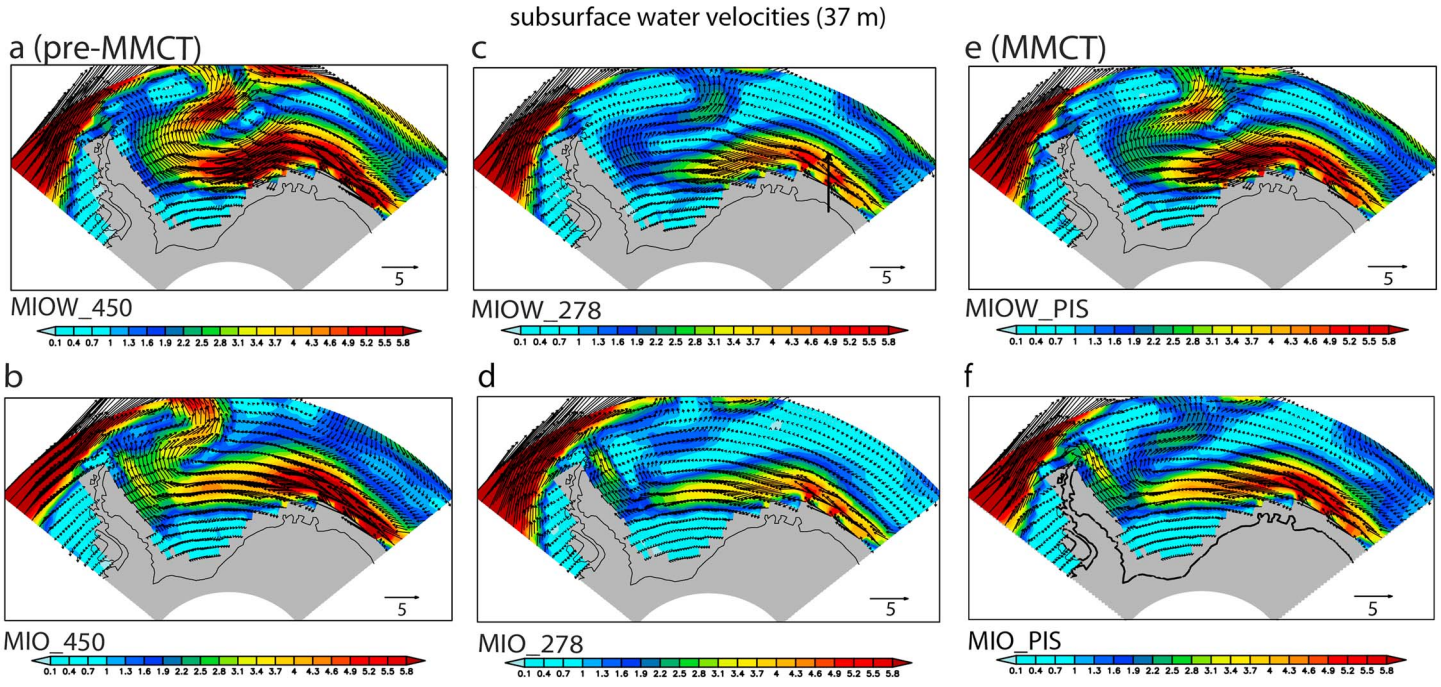

Figure 5. The simulated middle Miocene velocities ($cm\ s^{-1}$) in the Weddell Sea at surface (37 m) according to the six model experiments (MIOW_450, MIO_450, MIOW_278, MIO_278, MIOW_PIS, and MIO_PIS).

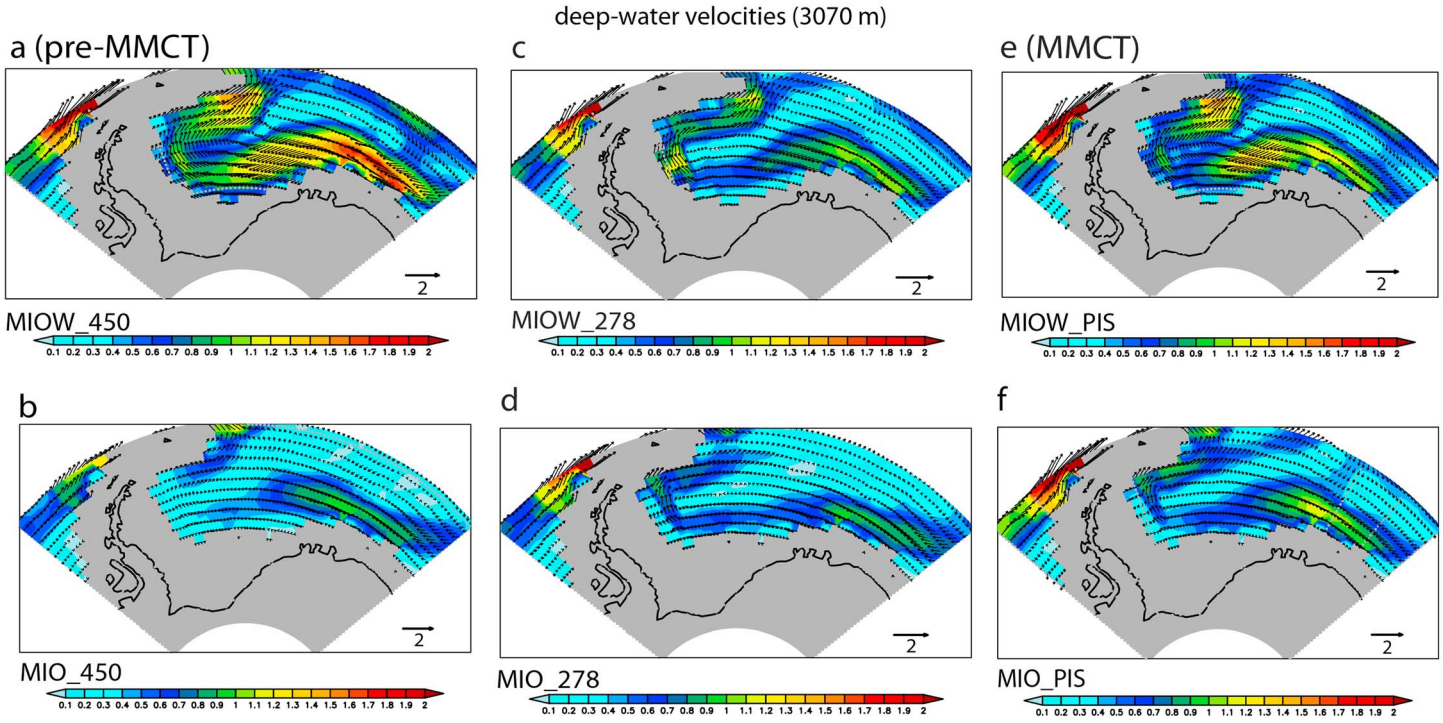

Figure 6. The simulated middle Miocene velocities (cm s^{-1}) in the Weddell Sea at depth 3070 m.

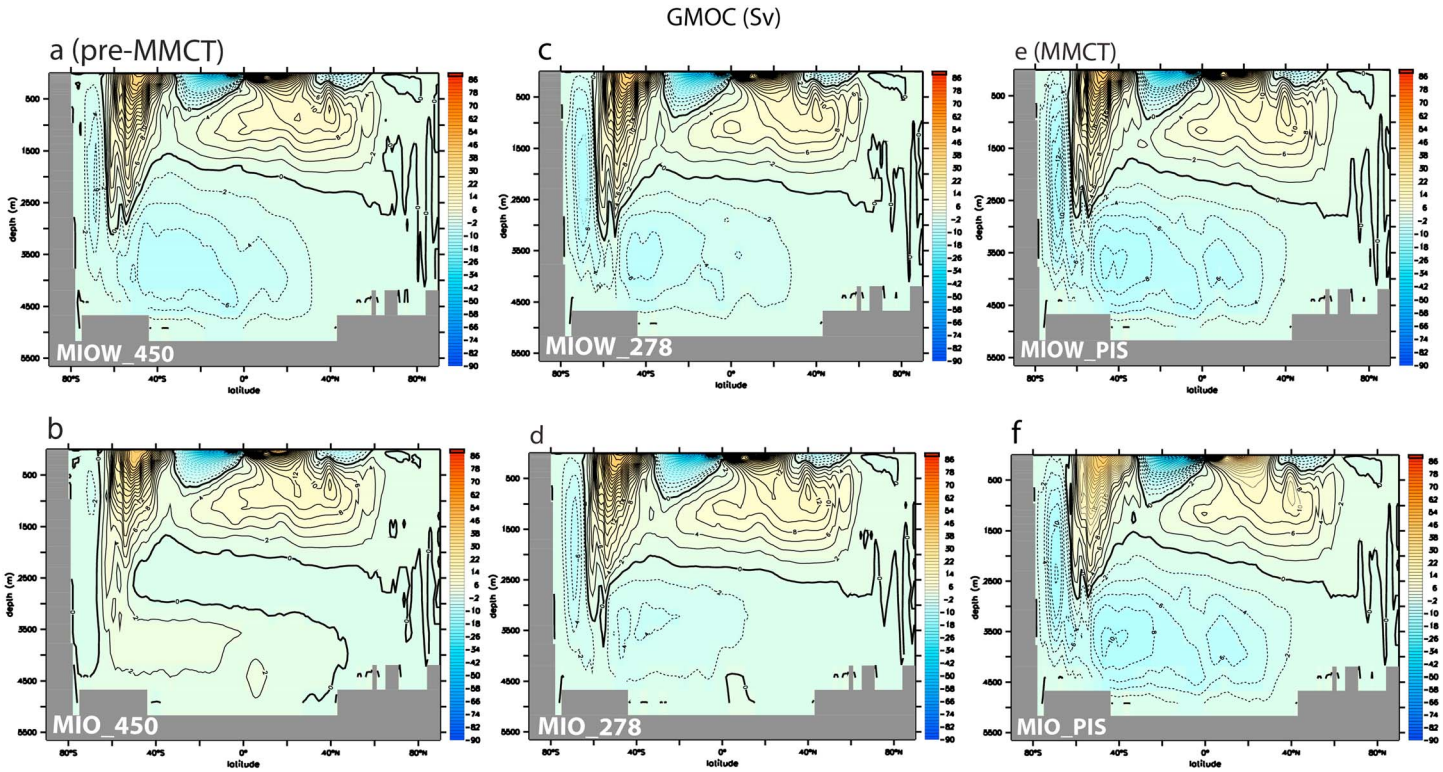

Figure 7. GMOC (Global Meridional Overturning Circulation) for the experiments of MIOW_450, MIO_450, MIO, MIOW_278, MIO_278, MIOW_PIS, and MIO_PIS.

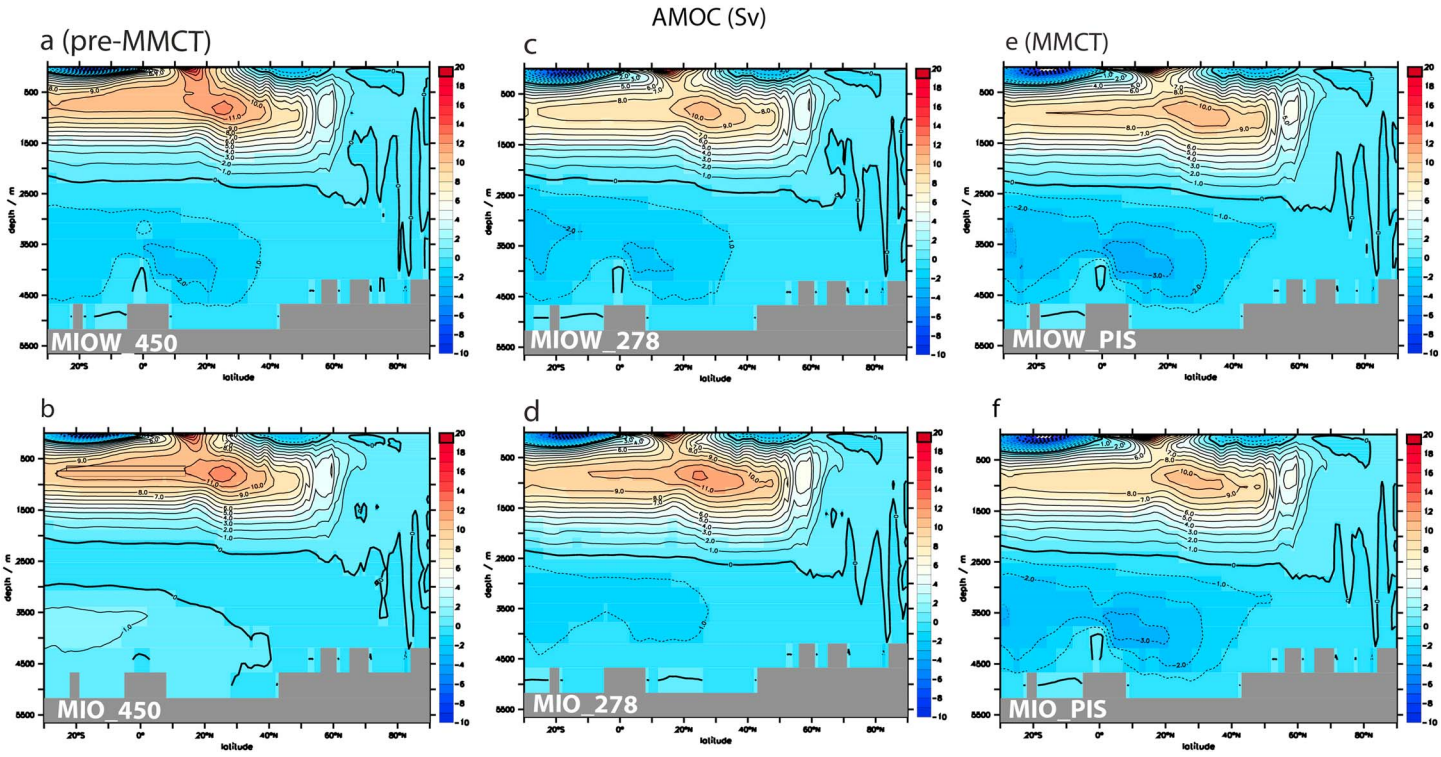

Figure 8. As Figure 7 but for AMOC (Atlantic Meridional Overturning Circulation).

between 2500 and 4600 m. The strength of the AABW index (defined as the strength of the stream function at ~30.5°S in the Atlantic) has a mean value of −1.98 (Table 2). In comparison to MIOW_450, the model experiment MIO_450 provides no deep water formation and a reversal AABW inflow as seen in both the AMOC (the mean value decreases to +0.77 Sv) and GMOC (the mean values decreases to −2.37 Sv) (Figures 7b and 8b and Table 2).

3.2. Effects of CO_2 Changes for Different Shelf Break Locations With a Low Ice Sheet

The progradation of the shelf break at relatively low atmospheric CO_2 concentration of 278 ppm causes profound changes in the ocean circulation, according to our model experiments (Figures 2c, 2d, 8c, and 8d). In both model experiments MIOW_278 and MIO_278, the Weddell Sea SSTs decline by at least 6°C as compared to the model experiments with high atmospheric CO_2 levels (MIOW_450 and MIO_450), representing the subsequent cooling after the pre-MMCT (Figures 2c and 2d). Along with a decline of CO_2, the mixed layer depth increases to a large extent, particularly in the Ross Sea sector and southern Weddell Sea (Figures 3c and 3d), and a robust deep water circulation is shown in both MIOW_278 and MIO_278 (Figures 6c and 6d). Reducing atmospheric CO_2 levels induce pronounced anomalous cooling around Antarctica that is likely due to increased sea ice cover and the associated ice-albedo feedback. The choice

Table 2. Antarctic Bottom Water (AABW) Index, as Defined by the Meridional Circulation in the Southern Ocean Between 60 and 80°S and Atlantic Ocean 30.5°S[a]

Model Runs	Global AABW Index (60–80°S, Sv)	AABW Index (Atlantic Inflow at 30.5°S, Sv)	Weddell Gyre Strength (Sv)
MIO_450	−2.37	−0.77	52
MIOW_450	**−6.5**	**−1.98**	**59**
MIOW_278	−9.4	−2.4	40
MIO_278	−7.1	−1.69	33
MIOW_PIS	**−12.**	**−3.2**	**52**
MIO_PIS	−12.2	−3.13	46

[a]Boldface is applied to highlight the values of interested time periods.

of Weddell Sea shelf slope position impacts the strength of Atlantic AABW at high CO_2 level; however, performing identical model simulations at low CO_2 levels yields smaller changes in the strength of Atlantic AABW (Figures 8a–8d). In addition, the isolated decline of atmospheric CO_2 from 450 to 278 ppmv (MIOW_450 and MIOW_278) provides only a small increase of about 0.42 Sv for the Atlantic AABW index (Figures 8b and 8d and Table 2).

3.3. Effect of Ice Sheets Growth for Different Shelf Break Locations With Low CO_2

In our model experiments with low atmospheric CO_2 concentrations, we further test the sensitivity of ocean circulation to ice sheet height changes, in particular by implementing the preindustrial ice sheet. In such a model setup, we aim to analyze the climate response with respect to the establishment of a fully developed Antarctic Ice Sheet during the MMCT (Figures 2e, 2f, 8e, and 8f). The model experiments with a fully developed Antarctic Ice Sheet show distinct global cooling compared to pre-MMCT (MIOW_450), and the cooling is accompanied by major increase in seasonal and perennial sea ice cover in the Southern Ocean (Figures 2a, 2b, 2e, and 2f). Similar to the shelf break effect at high CO_2 (see section 3.1), the northward migrated shelf break at low CO_2 also induces a consistent weakening of the Weddell Gyre circulation of about 7 Sv (Figure 4 and Table 2).

The isolated effect of increasing the height of the Antarctic Ice Sheet does not significantly affect SSTs or perennial sea ice that covers large areas of the Weddell Sea and Ross Sea (Figures 2a, 2b, 2e, and 2f). However, by increasing the ice sheet height, the mixed layer depth continually deepens in the Weddell Sea as seen in both experiments MIOW_PIS and MIO_PIS (Figures 3e and 3f). Correspondingly, a relatively strong Weddell Gyre evolves, extending from the surface toward deep water levels (Figures 3e, 3f, 5e, 5f, 6e, and 6f). In combination, the decrease of atmospheric CO_2 and the development toward a present day like Antarctic Ice Sheet in our model experiments show considerably enhanced regional sea ice formation (Figures 2a–2d). The strength of the Weddell Gyre circulation increases along with the full establishment of an Antarctic Ice Sheet (Figures 5d–5f and 6d–6f and Table 2).

Within all model experiments, the AABW reveals strongest sensitivity of all water masses. Herewith, maximum AABW formation takes place in both of the experiments MIO_PIS and MIOW_PIS, including a fully developed preindustrial Antarctic Ice Sheet configuration (Figures 7, 8e, and 8f). Thereby, the strength of AABW inflow into the Atlantic sector does not provide strong sensitivity with respect to the location of the shelf break at a fully developed Antarctic Ice Sheet (Figures 8c–8f).

4. Discussion

Proxy data from geological deep-sea records, such as $\delta^{18}O$ and $\delta^{13}C$, show that for the past 20 Ma, Antarctic temperatures have covaried with atmospheric CO_2 [*Pagani et al*., 1999; *Zachos et al*., 2008; *Beerling and Royer*, 2011; *Foster et al*., 2012], although the relationship may not be causal. Miocene atmospheric CO_2 appears poorly constrained and the low temporal resolution of the majority of the proxy records may not fully capture astronomically paced changes in atmospheric CO_2 [*Foster et al*., 2012; *Greenop et al*., 2014]. While considering these uncertainties, there is a growing consensus that atmospheric CO_2 varied between 500 and 278 ppm during middle to late Miocene [*Kürschner et al*., 2008; *Foster et al*., 2012; *Zhang et al*., 2013; *Greenop et al*., 2014].

The onset of a permanent ice sheet in Antarctica, CO_2 concentrations, and shelf break progradation by marine sedimentation processes can have played an essential role in setting the long-term boundary conditions for ocean circulation and deep water formation that modulated shorter-term variations during the pre-MMCT and MMCT times. The deep circulation of the subpolar regime is the product of many different coupled processes and factors including sea ice formation, extent, and seasonality, surface buoyancy fluxes, meridional eddy transport, surface wind stress, stratification, mixed layer depth, and seasonality, as well as topographic steering and blocking [*Meijers*, 2014]. AABW formation varies significantly between models in terms of ice sheet volume, temperature, and salinity as well as the boundary conditions like vegetation [*Knorr et al*., 2011; *Lohmann et al*., 2015]. This variance is due to the difficulty in accurately representing the complex chain of interactions between water masses, sea ice, winds, bathymetry, and ice shelves/sheets that combine to drive AABW formation.

4.1. AABW Formation During pre-MMCT

A warming ocean was simulated by the model, with a relatively small ice sheet, which is consistent with the findings from the middle Miocene benthic foraminifera characterized by variable and high benthic foraminifera Mg/Ca [*Kürschner et al*., 2008; *Lear et al*., 2015]. Our model experiment simulates the pre-MMCT (17–15 Ma) climate, which was warm and characterized by low global ice volume, followed by a period of significant Antarctic ice accumulation at ~15–12 Ma according to isotope studies [*Miller et al*., 1991; *Flower and Kennett*, 1994; *Zachos et al*., 2008; *Mudelsee et al*., 2014] (Figure 1). The retreat of the ice sheet into the continental interior during the pre-MMCT would have resulted in a reduction of sea ice and warmer water temperatures along the coastline, leading to a reduction in AABW production. In our simulation for the pre-MMCT, the new paleobathymetric constraints with a southerly placed shelf break perhaps facilitate the entrainment of warmer and saltier water from the surrounding oceans (e.g., Indian Ocean sector) into the southern Weddell Sea embayment, leading to increased sea surface heat exchange and the ultimate loss of perennial sea ice, therefore enhancing the convection and mixing (Figure 3a and Table 2).

The pronounced barotropic flow (Figure 4 and Table 2) and mixing in the Weddell Gyre (Figures 5a and 6a) governs the vertical water mass transport, fostering local deep water and remote circulation (Figures 7a and 8a). The overturning circulation in the Pacific and Atlantic sectors is characterized by stronger mixing, which leads to enhanced bottom water and deep water production in the Weddell Sea and also in the Ross Sea (Figures 7 and 8a).

In the carbon and oxygen isotopes retrieved from deep-sea drill sites of the southwest Pacific, *Flower and Kennett* [1995] and *Wright and Miller* [1996] found an increased SCW (AABW) production during the middle Miocene after ~15.6 Ma. This further supports the results from our model experiment of MIOW_450 that generates a relatively strong overturning circulation in the Pacific and Atlantic sectors (Figure 7a). Our model results demonstrate that heat loss and salt gain at the ocean-ice interface are perhaps not the only primary mechanism for AABW formation, while the paleobathymetry controlled by regional sedimentation and tectonic processes cannot be neglected. Interbasinal offsets in benthic foraminiferal carbon isotopes further indicate that the early Miocene Southern Ocean received warm saline deep water sourced from low latitudes in the Tethyan region [*Woodruff and Savin*, 1989; *Wright et al*., 1991]. This warm saline water mass likely ceased in the MMCT, and the consequent reduction in meridional heat transport has been called up as a trigger for the ice sheet expansion in the middle Miocene [*Woodruff and Savin*, 1989; *Flower and Kennett*, 1995].

4.2. Enhanced AABW Formation During MMCT

Distinct increased vertical $\delta^{18}O$ gradients in deep-sea cores suggest a prominent Antarctic Ice Sheet expansion during MMCT [*Flower and Kennett*, 1995; *Hall et al*., 2003; *Holbourn et al*., 2005, 2007; *Tripati et al*., 2009]. The rapid expansion of the East Antarctic Ice Sheet at 13.8 Ma is associated with a sea level fall in the order of ~60 m [*Miller et al*., 2005; *Lear et al*., 2010, 2015]. By reducing atmospheric CO_2 from 450 ppm to 278 ppm, and coupled with global high ice volume (PIS: preindustiral ice sheet), the model simulation generates a significantly strengthening overturning circulation at high latitudes of the Southern Ocean and some influence at low latitudes (Figures 7 and 8e). Deepening of the mixed layer in the southwest Ross Sea and southeast Weddell Sea (Figure 3e) suggests that upward displacement of more saline waters from depth and their partial mixing with surface water along the Antarctic continental margin could have contributed to the higher densities required for the production of the AABW. However, in our study, the solely decline of atmospheric CO_2 level from 450 ppm to 278 ppm has a small impact on the distribution of deep water formation areas (Figures 7 and 8a–8d). This is also consistent with a modeling study performed for the Late Cretaceous by *Donnadieu et al*. [2016], showing that varying CO_2 levels induce only minor changes in the deep water formation.

Our model experiments further highlight that large cooling down of the temperatures and an increased influx of AABW intrude the Atlantic Ocean, reaching about 45°N (Figures 7e and 8e). The incursion presumably reflects enhanced bottom water and deep water production in the Weddell Sea and Ross Sea, as indicated in GMOC and AMOC. Sea ice can impact the thermohaline circulation because its formation progress releases salt that creates cold and very salty water as brines. For a cold climate simulation, sea ice increases all around the Antarctic continent, notably in front of the Ross and Ronne-Filchner ice shelves (Figures 2c–2f). Convection near the boundaries results in sinking of a mixture of salty, near-freezing shelf waters and subsurface waters to great depths or even to the ocean bottom to form AABW. Such

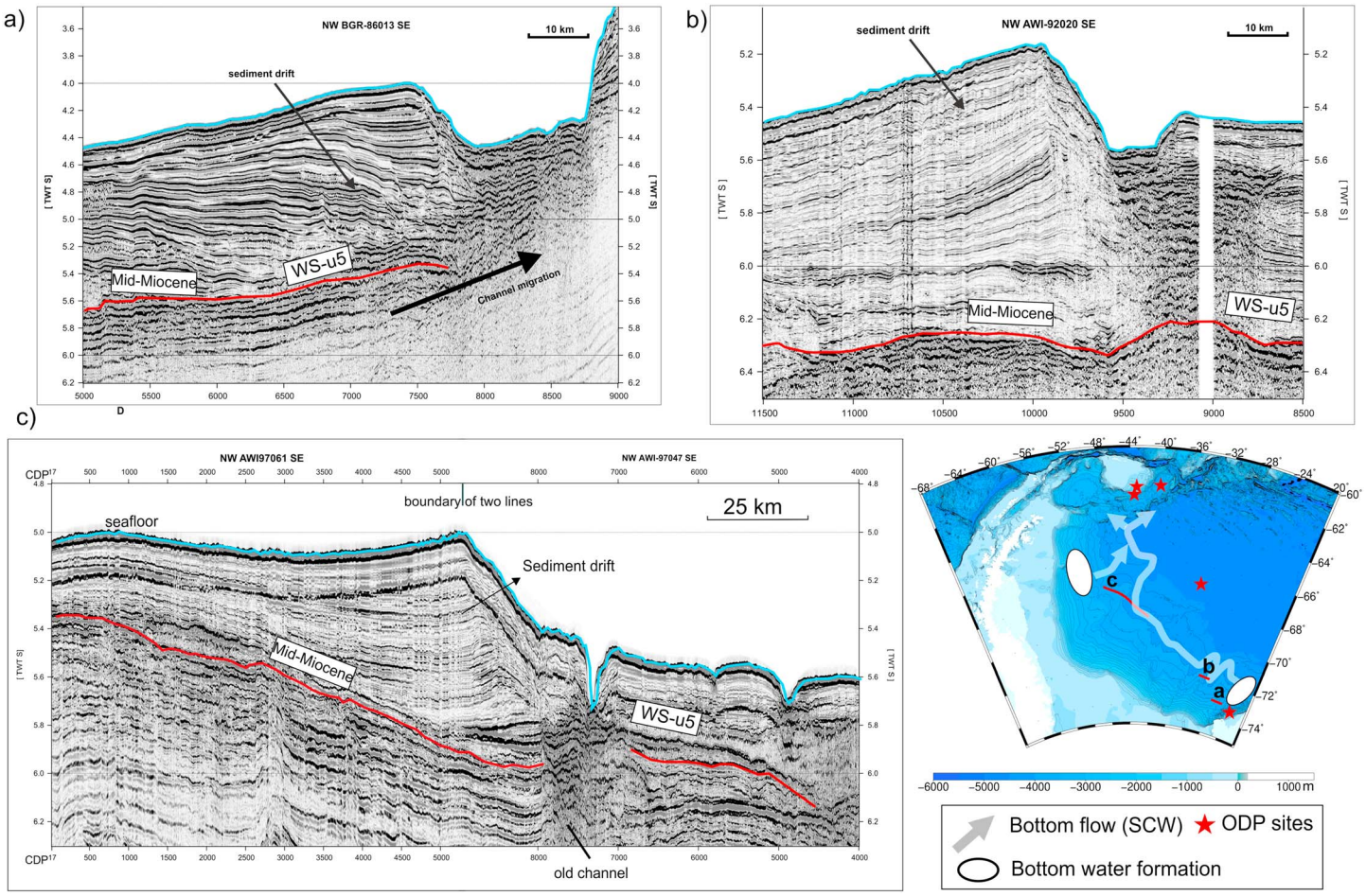

Figure 9. Sediment drifts examples in the Weddell Sea region and the basin-wide hiatus (WS_u5), which represents the middle Miocene. The location of the drift corresponds to the major deep water formation.

conditions favor local formation of AABW, which along with an increased AMOC would have affected climate in the middle Miocene through the global heat and moisture transports [*Sykes et al*., 1998; *Bice et al*., 2000]. The expansion of the Antarctic Ice Sheet near the coastlines would have contributed to colder surface water temperatures and expanded sea ice cover, which likely intensified the sinking of colder, denser water along the margins of Antarctica and resulted in the strengthening of AABW formation during periods when the ice was at its maximum (Figures 2e and 7e).

The modeling results mirror qualitatively previous findings from the India and Pacific sectors based on proxy studies that identified a major increase of SCW (AABW) production between 15.6 Ma and 12 Ma [*Woodruff and Savin*, 1989, 1991; *Flower and Kennett*, 1995]. They linked the increased production of deep and intermediate waters in the South Pacific to the cooling of Antarctica. Accompanied CO_2 decline with expanded Antarctic Ice Sheet and an ~6–7°C fall in sea surface temperature at high latitudes have certainly promoted the AABW formation during the MMCT.

Our model runs demonstrate that the improved paleobathymetry of the middle Miocene Weddell Sea causes the formation of modern-type deep water to spread to intermediate depths of the western Atlantic Ocean. Carbon isotope data compiled from sediment cores reveal a deep water source in the Atlantic sector of the Southern Ocean, which so far could not be matched in an ocean model experiment [*Butzin et al*., 2011]. The model experiment MIOW_PIS ppm with the improved Weddell Sea paleobathymetry (Table 1) is able to overcome the shortcomings of the above mentioned middle Miocene experiment study and to capture the southern source deep water contribution to the Atlantic overturning during the Neogene evolution of the modern ocean circulation.

4.3. Sedimentological-Geophysical Linkages

We argue that the intensified AABW originating in the Weddell Sea as well as the Weddell Gyre influenced the morphology of the continental rise by developing sediment drifts or contourites [*Rebesco et al*., 1997; *Hernández-Molina et al*., 2009; *Maldonado et al*., 2005; *Huang and Jokat*, 2016a, 2016b]. The dense and cold AABW, strong bottom currents, and intensified supply of glacially transported sediment to the continental rise are the prerequisites of developing these sediment drifts. Subsequent cooling after the pre-MMCT to the late Miocene, particularly during glacial periods, caused advances of the ice sheet across the shelf and ice streams pushing sediments onto the slope. The suspended components of slope deposits are part of turbidity currents, which become entrained in ambient bottom currents (AABW) forming large sediment drifts (Figure 9). A Weddell Sea basin-wide middle Miocene hiatus (WS-u5), identified from sediment cores of Ocean Drilling Project Site 693, correlates to the basis of these drifts [*Huang and Jokat*, 2016a] (Figure 9). This corresponds to the enhanced AABW formation during the MMCT according to our model experiment (Figures 7 and 8e). The sediments have been reworked by bottom currents and formed as drift bodies along the Weddell Sea margins since the middle Miocene.

5. Conclusions

By applying a fully coupled global atmosphere-ocean GCM, we examine the isolated impact of a Weddell Sea shelf break migration at high and low CO_2 levels to capture essential feedbacks between the climate system and sedimentological processes during middle Miocene times (pre-MMCT and MMCT). For the pre-MMCT, the model experiment shows that a more southerly placed shelf break in the southern Weddell Sea causes enhanced gyre transport and an increase of AABW formation in the Southern Ocean. The overturning circulation in the Pacific and Atlantic sectors is characterized by stronger mixing, which leads to enhanced bottom water and deep water production in the Weddell Sea and also in the Ross Sea.

For the MMCT, the model results further demonstrate that a CO_2 decrease leads to a temperature decrease independent of the shelf break position. In the case when the shelf break is in the northerly position an increased influx of AABW to the Atlantic Ocean is detected. On the contrary, the impact of CO_2 changes on AABW changes is comparatively small if the shelf break is in the southerly position. Furthermore, the different modeling scenarios show that an expansion of Antarctic Ice Sheet acts as the major forcing factor in promoting AABW formation. In future modeling studies with interactive ice sheet components it will be interesting to test whether the shelf progradation provides a stabilizing (positive) long-term feedback on Antarctic Ice Sheet growth. Such efforts should be complemented by enhanced bathymetry reconstructions of Antarctic embayment, with special emphasis on the Ross Sea sector, which also represents a key player for global-scale deep water formation.

Acknowledgments
X. Huang and M. Stärz made equal contributions to the study. The authors would like to thank the masters, crews, and seismic teams of the many ship expeditions to the Weddell Sea who made the acquisition of the seismic data used in this study possible. Comments by Torsten Bickert improved the manuscript. This study has primarily been supported through institutional funds of the Alfred Wegener Institute through Work Package 3.2 of its research program PACES-II. Data from this study are available through the NOAA NCDC online database (https://www.ncdc.noaa.gov), and additional data may be obtained from X.H. (Xiaoxia.huang@awi.de).

References

Barker, P. F., J. P. Kennett, and P. Scientific (1988), Weddell Sea palaeoceanography: Preliminary results of ODP leg 113, *Palaeogeogr. Palaeoclimatol. Palaeoecol.*, *67*(1), 75–102, doi:10.1016/0031-0182(88)90123-X.

Bart, P. J. (2003), Were West Antarctic ice sheet grounding events in the Ross Sea a consequence of East Antarctic ice sheet expansion during the middle Miocene?, *Earth Planet. Sci. Lett.*, *216*(1), 93–107, doi:10.1016/S0012-821X(03)00509-0.

Beerling, D. J., and D. L. Royer (2011), Convergent Cenozoic CO_2 history, *Nat. Geosci.*, *4*(7), 418–420, doi:10.1038/ngeo1186.

Bice, K. L., Scotese, C. R., Seidov, D., and Barron, E. J. (2000). Quantifying the role of geographic change in Cenozoic ocean heat transport using uncoupled atmosphere and ocean models, *Palaeogeogr. Palaeoclimatol. Palaeoecol.*, *161*(3), 295–310. doi:10.1016/S0031-0182(0182(00)00072-9.

Brovkin, V., T. Raddatz, C. H. Reick, M. Claussen, and V. Gayler (2009), Global biogeophysical interactions between forest and climate, *Geophys. Res. Lett.*, *36*, L07405, doi:10.1029/2009GL037543.

Butzin, M., G. Lohmann, and T. Bickert (2011), Miocene ocean circulation inferred from marine carbon cycle modeling combined with benthic isotope records, *Paleoceanography*, *26*, PA1203, doi:10.1029/2009PA001901.

Chow, J. M., and P. J. Bart (2003), West Antarctic Ice Sheet grounding events on the Ross Sea outer continental shelf during the middle Miocene, *Palaeogeogr. Palaeoclimatol. Palaeoecol.*, *198*(1), 169–186, doi:10.1016/S0031-0182(03)00400-0.

Cooper, A. K., G. Brancolini, C. Escutia, Y. Kristoffersen, R. Larter, G. Leitchenkov, P. O'Brien, and W. Jokat (2008), Cenozoic climate history from seismic reflection and drilling studies on the Antarctic continental margin, *Dev. Earth Environ. Sci.*, *8*, 115–234, doi:10.1016/S1571-9197(08)00005-0.

Dutton, J. F., and E. J. Barron (1997), Miocene to present vegetation changes: A possible piece of the Cenozoic cooling puzzle, *Geology*, *25*(1), 39–41.

Donnadieu, Y., E. Pucéat, M. Moiroud, F. Guillocheau, and J. F. Deconinck (2016), A better-ventilated ocean triggered by Late Cretaceous changes in continental configuration, *Nat. Commun.*, *7*, 10316, doi:10.1038/ncomms10316.

Ehlers, B. M., and W. Jokat (2013), Paleo-bathymetry of the northern North Atlantic and consequences for the opening of the Fram Strait, *Mar. Geophys. Res.*, *34*(1), 25–43, doi:10.1007/s11001-013-9165-9.

Flower, B. P., and J. P. Kennett (1994), The middle Miocene climatic transition: East Antarctic ice sheet development, deep ocean circulation and global carbon cycling, *Palaeogeogr. Palaeoclimatol. Palaeoecol.*, *108*(3–4), 537–555, doi:10.1016/0031-0182(94)90251-8.
Flower, B. P., and J. P. Kennett (1995), Middle Miocene deepwater paleoceanography in the southwest Pacific: Relations with East Antarctic Ice Sheet development, *Paleoceanography*, *10*(6), 1095–1112, doi:10.1029/95PA02022.
Foster, G. L., C. H. Lear, and J. W. Rae (2012), The evolution of pCO_2, ice volume and climate during the middle Miocene, *Earth Planet. Sci. Lett.*, *341*, 243–254, doi:10.1016/j.epsl.2012.06.007.
Gohl, K., G. Uenzelmann-Neben, R. D. Larter, C.-D. Hillenbrand, K. Hochmuth, T. Kalberg, E. Weigelt, B. Davy, G. Kuhn, and F.-O. Nitsche (2013), Seismic stratigraphic record of the Amundsen Sea Embayment shelf from pre-glacial to recent times: Evidence for a dynamic West Antarctic ice sheet, *Mar. Geol.*, *344*, 115–131, doi:10.1016/j.margeo.2013.06.011.
Goldner, A., N. Herold, and M. Huber (2014), Antarctic glaciation caused ocean circulation changes at the Eocene-Oligocene transition, *Nature*, *511*(7511), 574–577, doi:10.1038/nature13597.
Gong, X., G. Knorr, G. Lohmann, and X. Zhang (2013), Dependence of abrupt Atlantic meridional ocean circulation changes on climate background states, *Geophys. Res. Lett.*, *40*, 3698–3704, doi:10.1002/grl.50701.
Greenop, R., G. L. Foster, P. A. Wilson, and C. H. Lear (2014), Middle Miocene climate instability associated with high-amplitude CO_2 variability, *Paleoceanography*, *29*, 845–853, doi:10.1002/2014PA002653.
Hall, I. R., I. N. McCave, R. Zahn, L. Carter, P. C. Knutz, and G. P. Weedon (2003), Paleocurrent reconstruction of the deep Pacific inflow during the middle Miocene: Reflections of East Antarctic Ice Sheet growth, *Paleoceanography*, *18*(2), 1040, doi:10.1029/2002PA000817.
Hamon, N., P. Sepulchre, V. Lefebvre, and G. Ramstein (2013), The role of eastern Tethys seaway closure in the Middle Miocene Climatic Transition (ca. 14 Ma), *Clim. Past*, *9*(6), 2687–2702, doi:10.5194/cp-9-2687-2013.
Hayes, D. E., C. Zhang, and R. A. Weissel (2009), Modeling paleobathymetry in the Southern Ocean, *Eos. Trans. AGU*, *90*(19), 165–166, doi:10.1029/eost2009EO19.
Hernández-Molina, F. J., M. Paterlini, R. Violante, P. Marshall, M. de Isasi, L. Somoza, and M. Rebesco (2009), Contourite depositional system on the Argentine Slope: An exceptional record of the influence of Antarctic water masses, *Geology*, *37*(6), 507–510.
Herold, N., M. Seton, R. D. Müller, Y. You, and M. Huber (2008), Middle Miocene tectonic boundary conditions for use in climate models, *Geochem. Geophys. Geosyst.*, *9*, Q10009, doi:10.1029/2008GC002046.
Holbourn, A., W. Kuhnt, M. Schulz, and H. Erlenkeuser (2005), Impacts of orbital forcing and atmospheric carbon dioxide on Miocene ice-sheet expansion, *Nature*, *438*(7067), 483–487, doi:10.1038/nature04123.
Holbourn, A., W. Kuhnt, M. Schulz, J. A. Flores, and N. Andersen (2007), Orbitally-paced climate evolution during the middle Miocene "Monterey" carbon-isotope excursion, *Earth Planet. Sci. Lett.*, *261*(3), 534–550, doi:10.1016/j.epsl.2007.07.026.
Huang, X., and W. Jokat (2016a), Middle Miocene to present sediment transport and deposits in the Southeastern Weddell Sea, Antarctica, *Global Planet. Change*, *139*, 211–225, doi:10.1016/j.gloplacha.2016.03.002.
Huang, X., and W. Jokat (2016b), Sedimentation and potential venting on the rifted continental margin of Dronning Maud Land, *Mar. Geophys. Res.*, *37*, 313–324, doi:10.1007/s11001-016-9296-x.
Huang, X., K. Gohl, and W. Jokat (2014), Variability in Cenozoic sedimentation and paleo-water depths of the Weddell Sea basin related to pre-glacial and glacial conditions of Antarctica, *Global Planet. Change*, *118*, 25–41, doi:10.1016/j.gloplacha.2014.03.010.
Jungclaus, J. H., N. Keenlyside, M. Botzet, H. Haak, J. J. Luo, M. Latif, J. Marotzke, U. Mikolajewicz, and E. Roeckner (2006), Ocean circulation and tropical variability in the coupled model ECHAM5/MPI-OM, *J. Clim.*, *19*(16), 3952–3972, doi:10.1175/JCLI3827.1.
Jungclaus, J. H., et al. (2010), Climate and carbon-cycle variability over the last millennium, *Clim. Past*, *6*, 723–737, doi:10.5194/cp-6-723-2010.
Kennedy, A. T., A. Farnsworth, D. J. Lunt, C. H. Lear, and P. J. Markwick (2015), Atmospheric and oceanic impacts of Antarctic glaciation across the Eocene-Oligocene transition, *Phil. Trans. R. Soc. A*, *373*(2054, 20140419), doi:10.1098/rsta.2014.0419.
Kennett, J. P., et al. (1975), Cenozoic paleoceanography in the southwest Pacific Ocean, Antarctic glaciation, and the development of the Circum-Antarctic Current, *Initial Rep. Deep Sea Drill. Proj.*, *29*, 1155–1169.
Knorr, G., and G. Lohmann (2014), Climate warming during Antarctic ice sheet expansion at the Middle Miocene transition, *Nat. Geosci.*, *7*, 376–381, doi:10.1038/ngeo2119.
Knorr, G., M. Butzin, A. Micheels, and G. Lohmann (2011), A warm Miocene climate at low atmospheric CO_2 levels, *Geophys. Res. Lett.*, *38*, L20701, doi:10.1029/2011GL048873.
Kürschner, W. M., Z. Kvaček, and D. L. Dilcher (2008), The impact of Miocene atmospheric carbon dioxide fluctuations on climate and the evolution of terrestrial ecosystems, *Proc. Natl. Acad. Sci. U.S.A.*, *105*(2), 449–453.
Langebroek, P. M., A. Paul, and M. Schulz (2009), Antarctic ice-sheet response to atmospheric CO_2 and insolation in the Middle Miocene, *Clim. Past*, *5*(4), 633–646, doi:10.5194/cp-5-633-2009.
Langebroek, P. M., A. Paul, and M. Schulz (2010), Simulating the sea level imprint on marine oxygen isotope records during the middle Miocene using an ice sheet–climate model, *Paleoceanography*, *25*, PA4203, doi:10.1029/2008PA001704.
Lear, C. H., E. M. Mawbey, and Y. Rosenthal (2010), Cenozoic benthic foraminiferal Mg/Ca and Li/Ca records: Towards unlocking temperatures and saturation states, *Paleoceanography*, *25*, PA4215, doi:10.1029/2009PA001880.
Lear, C. H., H. K. Coxall, G. L. Foster, D. J. Lunt, E. M. Mawbey, Y. Rosenthal, M. S. Sosdian, E. Thomas, and P. A. Wilson (2015), Neogene ice volume and ocean temperatures: Insights from infaunal foraminiferal Mg/Ca paleothermometry, *Paleoceanography*, *30*, 1437–1454, doi:10.1002/2015PA002833.
Lohmann, G., M. Pfeiffer, T. Laepple, G. Leduc, and J. H. Kim (2013), A model-data comparison of the Holocene global sea surface temperature evolution, *Clim. Past*, *9*, 1807–1839, doi:10.5194/cp-9-1807-2013.
Lohmann, G., M. Butzin, and T. Bickert (2015), Effect of vegetation on the Late Miocene ocean circulation, *J. Mar. Sci. Eng.*, *3*(4), 1311–1333, doi:10.3390/jmse3041311.
Maldonado, A., et al. (2005), Miocene to recent contourite drifts development in the northern Weddell Sea (Antarctica), *Global Planet. Change*, *45*(1), 99–129, doi:10.1016/j.gloplacha.2004.09.013.
Marsland, S. J., H. Haak, J. H. Jungclaus, M. Latif, and F. Röske (2003), The Max-Planck-Institute global ocean/sea ice model with orthogonal curvilinear coordinates, *Ocean Model.*, *5*(2), 91–127, doi:10.1016/S1463-5003(02)00015-X.
Meijers, A. J. S. (2014), The Southern Ocean in the Coupled Model Intercomparison Project phase 5, *Philos. Trans. R. Soc. Lond. A: Math. Phys. Eng. Sci.*, *372*(2019, 20130296), doi:10.1098/rsta.2013.0296.
Micheels, A., A. A. Bruch, D. Uhl, T. Utescher, and V. Mosbrugger (2007), A late Miocene climate model simulation with ECHAM4/ML and its quantitative validation with terrestrial proxy data, *Palaeogeogr. Palaeoclimatol. Palaeoecol.*, *253*, 251–270, doi:10.1016/j.palaeo.2007.03.042.
Miller, K. G., J. D. Wright, and R. G. Fairbanks (1991), Unlocking the ice house: Oligocene-Miocene oxygen isotopes, eustasy, and margin erosion, *J. Geophys. Res.*, *96*(B4), 6829–6848, doi:10.1029/90JB02015.

Miller, K. G., M. A. Kominz, J. V. Browning, J. D. Wright, G. S. Mountain, M. E. Katz, P. J. Sugarman, B. S. Cramer, N. Christie-Blick, and S. F. Pekar (2005), The Phanerozoic record of global sea-level change, *Science*, *310*(5752), 1293–1298, doi:10.1126/science.1116412.

Mudelsee, M., T. Bickert, C. H. Lear, and G. Lohmann (2014), Cenozoic climate changes: A review based on time series analysis of marine benthic $\delta^{18}O$ records, *Rev. Geophys.*, *52*, 1–42, doi:10.1002/2013RG000440.

Pagani, M., K. H. Freeman, and M. A. Arthur (1999), Late Miocene atmospheric CO_2 concentrations and the expansion of C_4 grasses, *Science*, *285*(5429), 876–879, doi:10.1126/science.285.5429.876.

Pagani, M., J. C. Zachos, K. H. Freeman, B. Tipple, and S. Bohaty (2005), Marked decline in atmospheric carbon dioxide concentrations during the Paleogene, *Science*, *309*, 600–603.

Ramsay, A. T., C. W. Smart, and J. C. Zachos (1998), A model of early to middle Miocene deep ocean circulation for the Atlantic and Indian Oceans, *Geol. Soc. London Spec. Publ.*, *131*(1), 55–70.

Raymo, M. E. (1994), The initiation of Northern Hemisphere glaciation, *Annu. Rev. Earth Planet. Sci.*, *22*, 353–383.

Rebesco, M., R. D. Larter, P. F. Barker, A. Camerlenghi, and L. E. Vanneste (1997), History of sedimentation on the continental rise west of the Antarctic Peninsula, in *Geology and Seismic Stratigraphy on the Antarctic Margin: 2*, *Antarctic Research Series*, vol. 71, edited by A. K. Cooper and P. F. Barker, pp. 29–49, AGU, Washington, D. C.

Roeckner, E. et al. (2003), The Atmospheric General Circulation Model ECHAM5: Part 1. Model Description, Report No. 349, Max-Planck-Institut für Meteorologie, Hamburg, Germany.

Shevenell, A. E., J. P. Kennett, and D. W. Lea (2004), Middle Miocene Southern Ocean cooling and Antarctic cryosphere expansion, *Science*, *305*(5691), 1766–1770, doi:10.1126/science.1100061.

Smith, T., and J. B. Anderson (2011), Seismic stratigraphy of the Joinville Platform: Implications for regional climate evolution, in *Tectonic, Climatic and Cryospheric Evolution of the Antarctic Peninsula*, edited by J. B. Anderson and J. S. Wellner, pp. 51–62, AGU, Washington, D. C.

Stärz, M., G. Lohmann, and G. Knorr (2016), The effect of a dynamic soil scheme on the climate of the mid-Holocene and the Last Glacial Maximum, *Clim. Past*, *12*, 151–170, doi:10.5194/cp-12-151-2016.

Stein, R., et al. (2016), Evidence for ice-free summers in the late Miocene central Arctic Ocean, *Nat. Commun.*, *7*, doi:10.1038/ncomms11148.

Sykes, T. J. S., A. T. S. Ramsay, and R. B. Kidd (1998), Southern hemisphere Miocene bottom-water circulation: A palaeobathymetric analysis, *Geol. Soc. London Spec. Publ.*, *131*(1), 43–54.

Tripati, A. K., C. D. Roberts, and R. A. Eagle (2009), Coupling of CO_2 and ice sheet stability over major climate transitions of the last 20 million years, *Science*, *326*(5958), 1394–1397.

Uenzelmann-Neben, G., and K. Gohl (2012), Amundsen Sea sediment drifts: Archives of modifications in oceanographic and climatic conditions, *Mar. Geol.*, *299–302*, 51–62, doi:10.1016/j.margeo.2011.12.007.

Wei, W., and G. Lohmann (2012), Simulated Atlantic multidecadal oscillation during the Holocene, *J. Clim.*, *25*(20), 6989–7002, doi:10.1175/JCLI-D-11-00667.1.

Westerhold, T., T. Bickert, and U. Röhl (2005), Middle to late Miocene oxygen isotope stratigraphy of ODP site 1085 (SE Atlantic): New constrains on Miocene climate variability and sea-level fluctuations, *Palaeogeogr. Palaeoclimatol. Palaeoecol.*, *217*(3), 205–222, doi:10.1016/j.palaeo.2004.12.001.

Woodruff, F., and S. M. Savin (1989), Miocene deepwater oceanography, *Paleoceanography*, *4*(1), 87–140, doi:10.1029/PA004i001p00087.

Woodruff, F., and S. M. Savin (1991), Mid-Miocene isotope stratigraphy in the deep sea: High-resolution correlations, paleoclimatic cycles, and sediment preservation, *Paleoceanography*, *6*, 755–806, doi:10.1029/91PA02561.

Wright, J. D., and K. G. Miller (1996), Control of North Atlantic deep water circulation by the Greenland-Scotland Ridge, *Paleoceanography*, *11*(2), 157–170, doi:10.1029/95PA03696.

Wright, J. D., K. G. Miller, and R. G. Fairbanks (1991), Evolution of modern deepwater circulation: Evidence from the late Miocene Southern Ocean, *Paleoceanography*, *6*(2), 275–290, doi:10.1029/90PA02498.

You, Y., M. Huber, R. D. Müller, C. J. Poulsen, and J. Ribbe (2009), Simulation of the middle Miocene climate optimum, *Geophys. Res. Lett.*, *36*, L04702, doi:10.1029/2008GL036571.

Zachos, J. C., G. R. Dickens, and R. E. Zeebe (2008), An early Cenozoic perspective on greenhouse warming and carbon-cycle dynamics, *Nature*, *451*(7176), 279–283.

Zhang, X., G. Lohmann, G. Knorr, and C. Purcell (2014), Abrupt glacial climate shifts controlled by ice sheet changes, *Nature*, *512*, 290–294, doi:10.1038/nature13592.

Zhang, Y. G., M. Pagani, Z. Liu, S. M. Bohaty, and R. Deconto (2013), A 40-million-year history of atmospheric CO_2, *Philos. Trans. R. Soc. London, Ser. A*, *371*(2001), 20130096, doi:10.1098/rsta.2013.0096.